HHS Public Access

Author manuscript

Cancer Prev Res (Phila). Author manuscript; available in PMC 2015 October 01.

Published in final edited form as:

Cancer Prev Res (Phila). 2014 October ; 7(10): 1035–1044. doi:10.1158/1940-6207.CAPR-14-0097.

Widefield optical imaging of changes in uptake of glucose and tissue extracellular pH in head and neck cancer

Zhen Luo[1], **Melissa N. Loja**[2], **D. Greg Farwell**[3], **Quang C. Luu**[3], **Paul J. Donald**[3], **Deborah Amott**[3], **Anh Q. Truong**[3], **Regina Gandour-Edwards**[4], and **Nitin Nitin**[1,5]

[1]Department of Biological and Agricultural Engineering, University of California - Davis

[2]Department of Surgery, Division of Vascular Surgery, University of California - Davis

[3]Department of Otolaryngology, University of California - Davis

[4]Department of Pathology and Laboratory Medicine, University of California - Davis

[5]Food Science and Technology, University of California - Davis

Abstract

The overall objective of this study is to develop an optical imaging approach to simultaneously measure altered cell metabolism and changes in tissue extracellular pH with the progression of cancer using clinically isolated biopsies. In this study, 19 pairs of clinically normal and abnormal biopsies were obtained from consenting head and neck cancer patients at UCDMC. Fluorescence intensity of tissue biopsies before and after topical delivery of 2-NBDG (2-[N-(7-nitrobenz-2-oxa-1,3-diazol-4-yl)amino]-2-deoxy-D-glucose) and Alexa 647-pHLIP (pH (low) insertion peptide) was measured non-invasively by widefield imaging, and correlated with pathological diagnosis. The results of widefield imaging of clinical biopsies demonstrated that 2-NBDG and pHLIP peptide can accurately distinguish the pathologically normal and abnormal biopsies. The results also demonstrated the potential of this approach to detect sub-epithelial lesions. Topical application of the contrast agents generated a significant increase in fluorescence contrast (3–4 fold) in the cancer biopsies as compared to the normal biopsies, irrespective of the patient and location of the biopsy within a head and neck cavity. This unpaired comparison across all the cancer patients in this study highlights the specificity of the imaging approach. Furthermore, the results of this study indicated that changes in intracellular glucose metabolism and cancer acidosis are initiated in the early stages of cancer and these changes are correlated with the progression of the disease. In conclusion, this novel optical molecular imaging approach to measure multiple biomarkers in cancer has a significant potential to be a useful tool for improving early detection and prognostic evaluation of oral neoplasia.

Corresponding Author: N. Nitin, University of California, Davis, Department of Biological Engineering, One Shields Avenue, Davis, CA 95616, 530-752-6208, nnitin@ucdavis.edu.

Authors declare no conflicts of interest.

Introduction

Head and neck cancers continue to be the 6th most common cancer worldwide with approximately 270,000 new oral cavity tumors per year (1). Invasive procedures such as tissue and lymph node biopsies are the standard approaches used for clinical diagnosis and staging of the head and neck cancers (2, 3). There is a need to develop non-invasive molecular imaging approaches to aid in early detection, prognostic assessment, and subsequent longitudinal surveillance after treatment of the disease. Success in clinical translation of these imaging approaches will also enable molecular classification of the disease that may further improve detection sensitivity and/or prognostic assessment of the disease.

To develop a comprehensive molecular imaging approach to aid in detection and prognostic evaluation of head and neck cancers, this study evaluates simultaneous changes in metabolic activity of cells and acidosis in the extracellular domain using clinically isolated tissues. Upregulation of glucose metabolic pathways and a shift from aerobic metabolism to anaerobic metabolism (glycolysis) is the central hallmark of various cancers including breast, prostate, colon, head, and neck and is a sensitive indicator of progression of cancer (4, 5). The shift to glycolysis for energy production causes high rates of glucose consumption and also leads to a significant increase in production and release of acidic metabolites (such as protons and lactic acid) in the extracellular matrix (6, 7). Combined with the reduced capability of tumor-associated vasculature to deliver blood-based pH buffer, advanced cancers have an acidic extracellular pH as compared to normal tissue (8). Thus, the reduction of extracellular pH is a key hallmark of cancer progression and is closely associated with increased mutagenesis, metastasis, and resistance to radiation and drug therapies (9–16). Thus, measurement of simultaneous changes in metabolic activity and extracellular pH will have a significant impact on detection and prognosis of cancer and improve understanding of the correlation between changes in metabolic activity and acidosis in clinically isolated cancer biopsies.

Clinically, changes in glucose metabolic activity are measured by positron emission tomography (PET) using a radioactive glucose analog [18F]-fluoro-2-deoxyglucose (FDG). Currently, no clinical imaging approach is available for non-invasive measurement of changes in tissue pH with neoplasia. For imaging extracellular acidic environment in tumors, an experimental study using animal model system has investigated a pH-sensitive peptide-based PET imaging agent (17). This pH sensitive peptide inserts across the lipid bilayer at an acidic extracellular environment (pH<7.0) but not at a normal physiologic pH. In our recent study, we have demonstrated that topical application of fluorescently labeled pHLIP peptide can detect differences in extracellular pH in clinically abnormal and normal biopsies (18). Furthermore, currently there are no clinical imaging approaches for simultaneous measurement of molecular changes in metabolic activity and extracellular pH with the progression of cancer. Simultaneous measurements of multiple biomarkers in a clinical environment have a potential to improve detection specificity of oral neoplasia as demonstrated by a recent study (19).

Widefield fluorescence imaging was selected as the imaging modality in this study. Based on recent developments in optical instrumentation (20, 21), widefield optical imaging is emerging as a clinical approach to aid in detection of localized cancer lesions in head and neck cancer patients (19, 22). Furthermore, the widefield optical molecular in vivo imaging approaches are complementary to the whole body PET imaging. Similarly, widefield molecular imaging of ex vivo biopsy sample is complementary to the standard histology and immunohistochemistry (IHC) analysis of tissue sections by providing a rapid assessment of the isolated tissue without the need for sectioning and fixation (23).

In summary, the overall goal of this study was to develop optical molecular imaging approaches to simultaneously measure changes in multiple molecular biomarkers in clinically isolated head and neck biopsies. Evaluation using clinically isolated tissue samples is important as these clinical samples represent heterogeneity of disease among the population. Multiple imaging contrast probes (fluorescent glucose analog 2-NBDG and Alexa 647 labeled low pH insertion peptide pHLIP) were topically delivered to clinically isolated biopsy specimens, and the resulting contrast in clinically isolated tissues was measured using widefield fluorescence imaging.

Materials and Methods

(a) Probe selection and conjugation

Fluorescently labeled deoxyglucose (2-NBDG, 2-[N-(7-nitrobenz-2-oxa-1,3-diazol-4-yl)amino]-2-deoxy-D-glucose) was obtained from Invitrogen. For fluorescent labeling of the pHLIP peptide (ACEQNPIYWARYADWLFTTPLLLLDLALLVDADEGTG), Alexa Fluor® 647 C2 maleimide (Invitrogen) was reacted with the thiol (SH-group) of cysteine at the N-terminus of pHLIP to form a stable thioether bond. The details of the conjugation and purification process are described in our prior publication (18).

(b) Collection of paired biopsies

Pairs of clinically normal and abnormal biopsies (2mm–6mm in diameter) were obtained from patients who have signed informed consent and are undergoing surgical resection of suspected cancer at the University of California, Davis Medical Center (UCDMC). The paired biopsy samples were kept fresh in cold normal saline (0.9% NaCl), and were transported to the laboratory in less than 30 minutes.

(c) Widefield fluorescence imaging of tissue autofluorescence

To compare the increase in fluorescence intensity of topically labeled tissue samples, widefield fluorescent images before and after staining for each pair of biopsies were acquired. Pre-contrast images provide a measure of tissue autofluorescence background signal while the post-contrast images measure contributions from both autofluorescence and fluorescence of contrast media labeling. To assess autofluorescence before the application of fluorescent contrast media, the tissue was imaged using a commercially available widefield imaging system (Maestro 2, Cri (Woburn, MA) at the Center for Molecular and Genomic Imaging, University of California, Davis). For measuring autofluorescence of tissue biopsies in the 2-NBDG channel, the tissues were excited using a 500 nm wavelength light and the

fluorescence emission was collected using a 530–600 nm emission filter. For measuring autofluorescence of the tissue biopsies in the Alexa 647-pHLIP channel, the tissues were excited using a 640 nm wavelength light and the fluorescence emission was collected using a 670–800 nm emission filter. The integration time for the camera was maintained constant throughout the study at 100 ms.

(d) Topical labeling of intact biopsies

After autofluorescence imaging, both normal and abnormal paired biopsies were then topically labeled with 2-NBDG and Alexa 647-pHLIP simultaneously. The details of the topical labeling procedure and validation of delivery in biopsy tissues were described in our previously published research article (18). Probe delivery was achieved by topical labeling of isolated biopsy samples with 0.05 mg/ml 2-NBDG and 5 μM Alexa 647-pHLIP in non-buffered saline with 10% DMSO. After 60 minutes at 37° C, the biopsies were washed in normal saline for 10 minutes to remove any unbound 2-NBDG and Alexa 647-pHLIP.

(e) Post-contrast widefield fluorescence imaging

After removing unbound contrast agents (2-NBDG and Alexa 647-pHLIP) by washing tissue samples in normal saline, the tissue samples were again imaged by widefield imaging system using the same filter configurations for 2-NBDG and pHLIP-Alexa 647 as described in the previous section. Both the pre and post contrast images were acquired using the same integration time.

(f) Quantification of imaging data

For quantification of widefield images collected using the Maestro 2 Imaging system (CRi, Woburn, MA), both the white light and fluorescence images of biopsy samples were analyzed using ImageJ (Public domain, NIH). The whole tissue area was firstly selected in white light image by drawing the region of interest (ROI) around the edge of the tissue (illustrated in supplementary Fig. S3). The selected region identified in the white light image was overlaid on the corresponding fluorescence image. The mean fluorescence intensity (MFI) of the selected region was then calculated using ImageJ. To compare the MFI between cancer and normal biopsy samples across all patients, the average MFI was calculated by averaging the MFI from all isolated biopsies from individual patients.

The changes in MFI before and after topical delivery of contrast agents in each biopsy samples was calculated as: $\Delta MFI = MFI_{Post\text{-}contrast} - MFI_{Pre\text{-}contrast}$

To compare the difference in ΔMFI between unpaired samples, the average ΔMFI of all cancer biopsy samples and average ΔMFI of all unpaired normal samples were calculated.

The differential contrast ratio based on the ΔMFI of the clinically abnormal biopsy and the paired clinically normal biopsy was calculated as: $Ratio = \Delta MFI_{Abnormal}/\Delta MFI_{Normal}$

Where $\Delta MFI_{Abnormal}$ = ΔMFI of the clinically abnormal biopsy sample; ΔMFI_{Normal} = ΔMFI of the paired clinically normal biopsy sample.

The quantified imaging results from fluorescence imaging were analyzed using Microsoft® Excel 2007 (Microsoft Inc., Bellevue, WA) and SAS® (version 9.1 SAS Inc., Cary NC). Student's t-test was used for evaluating statistical significance between the treatments.

(g) Pathological Diagnosis

The tissue biopsies were fixed after the post-contrast imaging of the tissues. The fixed tissues were submitted to the pathology department for slicing and hematoxylin and eosin (H&E) staining. The prepared slides were evaluated by a board certified pathologist at the University of California, Davis (Regina Gandour-Edwards). The results from fluorescence imaging measurements were correlated with the pathological diagnosis.

Results

Clinically isolated biopsies

Table 1 shows the diverse anatomical locations within the head and neck cavity from which the paired biopsies were isolated and their corresponding pathological diagnosis. Fourteen consenting patients at UCDMC provided 14 clinically normal biopsies and 19 distinct clinically abnormal biopsies. Patients ranged from 51 and 84 years old, and 75% were male. All of the patients were white and had no prior history of oropharyngeal carcinoma. When multiple abnormal biopsies were obtained, they were collected from the same anatomical region but distinct locations within the tumor. The clinically isolated biopsies after evaluation with the selected molecular contrast probes were fixed, stained and evaluated by a board certified pathologist.

Widefield imaging of topically applied 2-NBDG and pHLIP in paired clinically normal and abnormal biopsies

The results in this section demonstrate simultaneous imaging of changes in glucose metabolic activity and extracellular pH in clinically isolated paired biopsies (Figure 1). Pre-contrast images were acquired before topical delivery of 2-NBDG to assess the autofluorescence signal intensity of each biopsy sample. Figure 1(A1) shows the results from a paired biopsy sample in which the clinically abnormal sample has a significantly lower autofluorescence signal intensity as compared to the corresponding clinically normal biopsy specimen. In the post contrast images (after topical delivery of 2-NBDG, Fig 1(A2)), the fluorescence signal from the clinically abnormal biopsy shows a significant increase in fluorescence contrast as compared to the paired clinically normal biopsy.

The MFI was calculated for both the clinically abnormal and normal biopsies before and after topical application of 2-NBDG (Fig 1(A3)). The MFI before staining represents the contribution from tissue autofluorescence, and the MFI after staining represents the contribution from both tissue autofluorescence and 2-NBDG uptake. Results demonstrate a substantial increase in fluorescence intensity of the clinically abnormal biopsy sample as compared to the clinically normal biopsy. Based on the pathology evaluation, the clinically abnormal biopsy was diagnosed as squamous cell carcinoma and the clinically normal biopsy was diagnosed as normal. Histological image of these clinically abnormal and normal biopsy are shown in Figure 1C.

Figure 1(B1 and B2) shows the representative widefield fluorescence images of the biopsy samples imaged using the emission wavelength range of 670–800 nm. This wavelength range was used for imaging tissue contrast generated upon binding of Alexa 647 labeled pHLIP peptide. Similar to the approach outlined for the 2-NBDG, the tissue biopsies were imaged prior to application of contrast agent to determine the background autofluorescence of the tissue in the wavelength range of 670–800nm (Fig 1(B1)). After topical delivery of pHLIP in tissue samples, substantial increase in fluorescence intensity was noticed in the clinically abnormal biopsy, while there was a small increase in fluorescence intensity of the clinically normal tissue (Fig 1(B2)).

Figure 1(B3) shows the MFI for the both the pre and post contrast widefield fluorescence images of clinically abnormal and normal biopsies. The quantified imaging results illustrate that the MFI increased significantly in the clinically abnormal biopsy as compared to the paired normal biopsy isolated from the same patient. Overall, the trend observed with 2-NBDG and pHLIP based contrast agents, shows selective and significant increase in fluorescence contrast in a clinically abnormal biopsy (pathological diagnosis: squamous cell carcinoma) as compared to the pathologically and clinically normal biopsy.

Differences in fluorescence contrast between clinically abnormal and normal biopsies were independent of the tissue autofluorescence levels

Changes in tissue autofluorescence induced by neoplasia have been used as an optical biomarker for detecting head and neck cancer (24–26). In many of the paired biopsy sets the autofluorescence signal intensity of the normal biopsy was higher than the paired abnormal biopsy. In contrast to this trend, the autofluorescence signal intensity of the certain clinically normal biopsies was lower than the paired clinically abnormal samples (n=5 in the 2-NBDG fluorescence channel and n=3 in the Alexa 647 fluorescence channel). Figures 2(A1 and B1) illustrates an example of a clinical case in which the autofluorescence signal intensity of the clinically and pathologically normal sample (pre-contrast) was lower than the autofluorescence intensity of the clinically and pathologically abnormal sample. However, another clinically abnormal biopsy sample taken from the same patient and from the same anatomical area shows lower autofluorescence intensity than the paired normal tissue (Fig 2(Cancer 2)). This data set indicates that the differences in autofluorescence can also be due to a variety of patho-physiological factors including neoplasia (25, 27).

Figure 2(A2 and B2) shows the post-contrast images of the paired biopsy sets from a patient (two clinically abnormal biopsies and one clinically normal biopsy). After topical delivery of 2-NBDG and pHLIP in the tissue samples, a substantial increase in fluorescence intensity was noticed in both the clinically abnormal biopsies, while there was a small increase in fluorescence intensity of the clinically normal tissue. The quantification of the MFI is shown in Figure 2(A3 and B3). The corresponding histology and pathological diagnosis for these biopsy samples is shown in Figure 2(C3). The results show that both the clinical abnormal biopsies were diagnosed as squamous cell carcinoma, and the clinically normal biopsy was diagnosed as pathologically normal. These results demonstrate that enhancement in fluorescence contrast resulting from specific uptake of 2-NBDG or binding of the pHLIP

peptide in diseased biopsy specimens is not significantly influenced by the native autofluorescence properties.

Sensitivity of 2-NBDG and pHLIP in detecting sub-surface lesions

Results in Figure 3 illustrate an example of a clinical case in which the clinically normal biopsy had invasive cancer underlying the normal epithelial tissue. The pre-contrast images of the paired biopsy set illustrate that the clinically normal biopsy has a lower autofluorescence signal in both the 2-NBDG and the Alexa 647-pHLIP emission channels as compared to clinically abnormal biopsy. After simultaneous topical labeling of the biopsies with 2-NBDG and Alexa 647-pHLIP, the post contrast images illustrate a significant increase in fluorescence contrast in both the clinically normal and abnormal biopsies as shown in Figure 3(A2 and B2). Based on the quantification of the MFI for pre and post contrast images, the results in Figure 3(A3) show that after staining with 2-NBDG, the MFI of the normal biopsy was similar to the MFI of the paired clinically abnormal biopsy. This is particularly significant since the MFI of the normal biopsy was lower than the paired abnormal biopsy in the pre-contrast images. Quantification of the MFI for the Alexa 647-pHLIP labeled biopsies in Figure 3(B3) also show a significant increase in the MFI of both the paired clinically abnormal and normal biopsies in the post contrast images.

Results of pathological analysis revealed that the clinically normal biopsy had an invasive cancer underneath the normal epithelial section (Fig 3(C3)). The histological analysis indicated that the invasive cancer covered over 2/3 width of the biopsy sample underlying a normal epithelium. In this case, the normal appearance of the tissue influenced the clinical impression of the tissue and without the biopsy it was not possible to clinically detect the presence of invasive disease.

Using a combination of topically applied contrast agents (both 2-NBDG and Alexa 647-pHLIP) and widefield fluorescence imaging, the optical imaging approach was able to detect disease underlying a normal epithelium. This result reflects that the combination of topically applied contrast agents and widefield imaging cannot only detect surface lesions, but also aid in detection of sub-surface lesions that are often difficult to detect based on visual impression of the tissue.

2-NBDG uptake and pHLIP binding across all cancerous biopsies

Figure 4A compares the average ΔMFI in cancer biopsies (i.e. the average increase of MFI between post- and pre-contrast images) with the normal biopsies across all cancer patients in this study irrespective of the anatomic location within the head and neck cavity. This analysis compares the increase in the mean fluorescence contrast based on uptake of 2-NBDG and binding of pHLIP peptide across all cancer and normal biopsies (i.e. the tissue samples are unpaired). Results showed the average ΔMFI of cancer biopsies (n=11) was significantly higher (approximately 2.5 and 3.3 fold) as compared to the average ΔMFI of normal biopsies (n=7; p=0.003) after topical delivery of 2-NBDG and pHLIP, respectively. These results demonstrate the potential of using fluorescence labeled glucose and pHLIP to distinguish clinically abnormal tissues from normal tissues across diverse patients by comparing the ΔMFI. The results of average MFI of all biopsy samples before (pre-contrast)

and after (post-contrast) topical delivery with 2-NBDG and pHLIP are shown in the Supplementary Data Figure S1.

Correlation between changes in 2-NBDG uptake and pHLIP binding with stages of neoplasia

To compare the changes in metabolic activity and extracellular activity with development of neoplasia, the average differential contrast ratio was calculated between the ΔMFI of pathologically abnormal biopsies with respect to the ΔMFI of paired normal biopsies. This average contrast ratio was calculated separately for the 2-NBDG and the Alexa 647-pHLIP and was plotted as a function of pathological diagnosis in Figure 4B.

The results show a multifold increase in the differential contrast ratio between the paired diseased and normal biopsies and the average contrast ratio increased with an increase in severity of the disease. The average contrast ratio for the cancer biopsies (n=9) was approximately 3 and 5.9 fold higher as compared to the pathological normal biopsies stained with 2-NBDG and Alexa 647-pHLIP respectively. For the carcinoma in-situ cases (n=2), the increase in ratiometric contrast was approximately 1.8 and 3.3 fold as compared to normal biopsies stained with 2-NBDG and Alexa 647-pHLIP respectively. For the dysplasia cases (n=2), the increase in ratiometric contrast was approximately 1.21 and 1.7 fold as compared to normal biopsies stained with 2-NBDG and Alexa 647-pHLIP respectively. Overall these results indicate that significant changes in both metabolic activity and extracellular pH can be detected in clinically abnormal biopsies as compared to the paired normal biopsies.. The results also show the pHLIP labeling does result in a relatively higher ratiometric contrast ratio in paired biopsy sets as compared to 2-NBDG at all stages of the disease.

In Figure 4B, the results also show the cases in which clinically abnormal biopsy were diagnosed as normal biopsy based on pathology evaluation. For the pathologically normal biopsies, despite appearing abnormal clinically, the ΔMFI of 2-NBDG uptake (n=3) and pHLIP binding (n=2) was similar to the ΔMFI of paired normal biopsies. These biopsies were further confirmed as normal based on the pathology review. These results demonstrate specificity of 2-NBDG and pHLIP based imaging approaches to distinguish true pathologically cancer biopsy from normal biopsies.

Discussion

Topical delivery of contrast agents enables molecular analysis of intact tissues

Topical delivery is a non-invasive approach to deliver molecular contrast agents to localized tissues. Topical delivery approach provides rapid access to the epithelial tissue and overcomes significant limitations of the alternative delivery approaches such intravenous delivery of contrast media. These limitations include non-specific retention of contrast agents in organs such as liver, kidney and delay in imaging time to allow for clearance of the contrast media from the circulation. The results of this study demonstrate that topical delivery of contrast agents to ex-vivo biopsies was an efficient approach for the delivery of both small molecular weight contrast agent (2-NBDG, MW: 342) and a short peptide (pHLIP, MW: 3000 Da). These results are in agreement with the results of our prior studies

(28, 29). Results in Figure 3 also demonstrate that the molecular contrast agents were able to target the sub-epithelial lesions using topical application. This result is also in agreement with the results presented in our recent study (18).

To translate topical delivery of contrast agents to in-vivo application in a clinical setting, further research is needed to develop topical oral formulations. It is desired that these topical formulations have mucoadhesive properties and provide rapid delivery of imaging contrast agents to target tissues. The mucoadhesive properties will enable localized application of the contrast agents at target sites within the head and neck cavity. In the current literature, various mucoadhesive formulations have been developed for the delivery of therapeutic molecules (30–32). The applications of these therapeutic molecules range from suppressing inflammation (32), prevention of cancer (30, 31) and treatment of localized infections (33) in the oral cavity. These topical delivery approaches provide a framework to adapt these concepts for the delivery of imaging contrast agents. To achieve rapid and uniform delivery of imaging agents, the existing topical formulations can be further modified to include triggered release mechanisms or rapidly eroding polymer formulations (34).

Specificity of 2-NBDG and pHLIP in detection of pre-cancerous and cancerous lesions

The results of this study demonstrate high specificity of both 2-NBDG and pHLIP in detection of both pre-cancerous and cancerous lesions. The specificity is highlighted by the facts that both the molecular contrast agents accurately distinguished the pathologically normal and abnormal biopsies. In this study, three biopsy samples that were considered as clinically abnormal based on the physical examination were found to be normal based on pathological diagnosis. In the evaluation of these paired biopsies using molecular contrast agents, the clinically abnormal appearing tissue (but pathologically normal) biopsies did not show a significant increase in fluorescence contrast as compared to the paired clinically and pathologically normal tissues. For further clinical translation, specificity of this approach for discriminating other clinical symptoms such as infections may be further evaluated.

Evaluation of paired biopsies using molecular contrast agents improved the specificity of detecting cancerous lesions as compared to their evaluation using pre-contrast imaging measurements only (autofluorescence properties).. Results show that the ratio of autofluorescence intensity of cancer biopsies with respect to the paired normal biopsy varied among patients and significant number of paired biopsy sets had autofluorescence ratio greater than one in both 2-NBDG and Alexa-647 channels. It is important to note that the primary focus of pre-contrast imaging measurements was to normalize variation in endogenous contrast among different tissue biopsies. Thus, the selected wavelengths for pre-contrast imaging may not be optimal (35) for detecting neoplasia based on autofluorescence properties of the tissues.

In this study, one of the clinically normal biopsy was also diagnosed as a cancer biopsy based on pathology evaluation. Pathological evaluation showed that the cancer was localized in the sub-epithelial tissue, while the epithelial section of the tissue had a normal anatomical structure. A significant change in fluorescence contrast properties was also observed upon topical application of contrast media in this clinically normal, but pathologically abnormal tissue. These results are significant as the imaging approaches may provide a unique method

to differentiate cancer tissue with normal epithelium (sub-epithelial cancers) which cannot be easily identified clinically.

The specificity of both the molecular contrast agents is also illustrated in the results of Figure 4A. This result compares the data set of cancer biopsies across all patients without any pairing of the biopsy specimens. The result show that even without pairing, the cancer biopsies showed a significantly higher (3 to 4 fold) higher increase in fluorescence contrast as compared to the normal biopsies. This trend is significant as this comparison is across diverse sites within the head and neck cavity and across diverse patients.

The results of this study also illustrate the potential of the selected molecular imaging probes to detect changes in the pre-cancerous stages (both dysplasia and carcinoma-in-situ) of head and neck cancer. Since the study was conducted at a tertiary care center, the number of biopsies at early stage of the disease is small as compared to the cancer biopsies. In order to further validate the sensitivity of the selected molecular contrast media to detect early stage biopsy samples, more biopsy samples from early stage patients are needed.

Correlation between metabolic activity and acidosis

The results of this study illustrate that upregulation in metabolic activity with development of neoplasia is correlated with acidosis in extracellular matrix of the tissue. This correlation was observed in both precancerous and cancerous lesions. Changes in both metabolic activity and extracellular pH in pre-cancerous lesions indicate that these molecular transformations are not only a result of changes in tissue vasculature in tumors but are present in early stages (avascular stage) of the disease. This evidence indicates that changes in gene expression associated with up regulated metabolic activity and acidosis such as activation of hypoxia pathway are triggered in early stages of the disease and these changes are significantly enhanced by the time disease becomes invasive. This evidence supports the discussion on the role of acidosis, hypoxia and glycolysis in progression of disease from dysplasia and carcinoma in-situ to invasive disease (36). This evidence is also supported by other studies that have indicated the role acidosis in extracellular tissue in promoting growth of tumors (37).

Conclusion

A novel optical molecular imaging approach was developed in this study based on simultaneous imaging of changes in glucose metabolic activity and extracellular pH in clinically isolated fresh biopsy specimens. The results of this study demonstrate high specificity of both the glucose and the pH imaging probes in detecting both early and late stages of the disease. The molecular imaging measurements correlated with the pathological diagnosis of the biopsy samples in all cases including early stages of the disease and were able to distinguish between cancer and normal biopsies across all patients and anatomical sites in the head and neck cavity. The results of this study indicate that changes in intracellular glucose metabolism and cancer acidosis are initiated in the early stages of the disease and these two selected biomarkers are correlated with the progression of the disease. Overall, based on the combination of widefield whole-tissue imaging and non-invasive topical application of the contrast media, the molecular imaging approach has significant

potential to aid in detection. Future research is required to evaluate the potential of this molecular imaging approach for prognostic assessment, tumor margin detection and monitoring of therapy response in a clinical environment.

Supplementary Material

Refer to Web version on PubMed Central for supplementary material.

Acknowledgments

This project described was supported by the National Center for Research Resources, Nation Institute of Health, through grant number UL1 RR024146 and linked award TL1 RR024145. The grant recipients are M. Loja and Z. Luo. Its contents are solely the responsibility of the authors and do not necessarily represent the official view of NCRR or NIH. Information on Re-engineering the Clinical Research Enterprise can be obtained from: http://nihroadmap.nih.gov/clinicalresearch/overview-translational.asp

References

1. Jemal A, Bray F, Center MM, Ferlay J, Ward E, Forman D. Global cancer statistics. CA Cancer J Clin. 2011; 61:69–90. [PubMed: 21296855]
2. Neville BW, Day TA. Oral cancer and precancerous lesions. CA Cancer J Clin. 2002; 52:195–215. [PubMed: 12139232]
3. Fleskens S, Slootweg P. Grading systems in head and neck dysplasia: their prognostic value, weaknesses and utility. Head Neck Oncol. 2009; 1:11. [PubMed: 19432960]
4. Glunde K, Artemov D, Penet MF, Jacobs MA, Bhujwalla ZM. Magnetic resonance spectroscopy in metabolic and molecular imaging and diagnosis of cancer. Chem Rev. 2010; 110:3043–59. [PubMed: 20384323]
5. Choy G, Choyke P, Libutti SK. Current advances in molecular imaging: noninvasive in vivo bioluminescent and fluorescent optical imaging in cancer research. Mol Imaging. 2003; 2:303–12. [PubMed: 14717329]
6. Gatenby RA, Gillies RJ. Why do cancers have high aerobic glycolysis? Nat Rev Cancer. 2004; 4:891–9. [PubMed: 15516961]
7. Denko NC. Hypoxia, HIF1 and glucose metabolism in the solid tumour. Nat Rev Cancer. 2008; 8:705–13. [PubMed: 19143055]
8. Wike-Hooley JL, Haveman J, Reinhold HS. The relevance of tumour pH to the treatment of malignant disease. Radiother Oncol. 1984; 2:343–66. [PubMed: 6097949]
9. Dellian M, Helmlinger G, Yuan F, Jain RK. Fluorescence ratio imaging of interstitial pH in solid tumours: Effect of glucose on spatial and temporal gradients. British Journal of Cancer. 1996; 74:1206–15. [PubMed: 8883406]
10. Gatenby RA, Gawlinski ET. The glycolytic phenotype in carcinogenesis and tumor invasion: Insights through mathematical models. Cancer Research. 2003; 63:3847–54. [PubMed: 12873971]
11. Gatenby RA, Gillies RJ. Glycolysis in cancer: a potential target for therapy. Int J Biochem Cell Biol. 2007; 39:1358–66. [PubMed: 17499003]
12. Buck AK, Herrmann K, Shen CX, Dechow T, Schwaiger M, Wester HJ. Molecular imaging of proliferation in vivo: Positron emission tomography with [F-18]fluorothymidine. Methods. 2009; 48:205–15. [PubMed: 19318128]
13. Jadvar H, Alavi A, Gambhir SS. 18F-FDG uptake in lung, breast, and colon cancers: molecular biology correlates and disease characterization. J Nucl Med. 2009; 50:1820–7. [PubMed: 19837767]
14. Niederkohr RD, Gamie SH. F-18FDG PET as an Imaging tool for detecting and staging metastatic basal-cell carcinoma. Clinical Nuclear Medicine. 2007; 32:491–2. [PubMed: 17515767]
15. Plathow C, Weber WA. Tumor cell metabolism imaging. Journal of Nuclear Medicine. 2008; 49:43S–63S. [PubMed: 18523065]

16. Visser EP, Philippens MEP, Kienhorst L, Kaanders J, Corstens FHM, de Geus-Oei LF, et al. Comparison of tumor volumes derived from glucose metabolic rate maps and SUV maps in dynamic F-18-FDG PET. Journal of Nuclear Medicine. 2008; 49:892–8. [PubMed: 18483085]
17. Vavere AL, Biddlecombe GB, Spees WM, Garbow JR, Wijesinghe D, Andreev OA, et al. A Novel Technology for the Imaging of Acidic Prostate Tumors by Positron Emission Tomography. Cancer Research. 2009; 69:4510–6. [PubMed: 19417132]
18. Loja MN, Luo Z, Farwell DG, Luu QC, Donald PJ, Amott D, et al. Optical molecular imaging detects changes in extracellular pH with the development of head and neck cancer. International Journal of Cancer. 2013; 132:1613–23.
19. Rosbach KJ, Williams MD, Gillenwater AM, Richards-Kortum RR. Optical molecular imaging of multiple biomarkers of epithelial neoplasia: epidermal growth factor receptor expression and metabolic activity in oral mucosa. Transl Oncol. 2012; 5:160–71. [PubMed: 22741035]
20. Bedard N, Pierce M, El-Nagger A, Anandasabapathy S, Gillenwater A, Richards-Kortum R. Emerging roles for multimodal optical imaging in early cancer detection: a global challenge. Technol Cancer Res Treat. 2010; 9:211–7. [PubMed: 20218743]
21. McWilliams A, MacAulay C, Gazdar AF, Lam S. Innovative molecular and imaging approaches for the detection of lung cancer and its precursor lesions. Oncogene. 2002; 21:6949–59. [PubMed: 12362276]
22. Pierce MC, Richards-Kortum R. Low-cost, portable optical imaging systems for cancer diagnosis. Conf Proc IEEE Eng Med Biol Soc. 2010; 2010:1093–6. [PubMed: 21096559]
23. Pierce MC, Javier DJ, Richards-Kortum R. Optical contrast agents and imaging systems for detection and diagnosis of cancer. Int J Cancer. 2008; 123:1979–90. [PubMed: 18712733]
24. Betz CS, Mehlmann M, Rick K, Stepp H, Grevers G, Baumgartner R, et al. Autofluorescence imaging and spectroscopy of normal and malignant mucosa in patients with head and neck cancer. Lasers Surg Med. 1999; 25:323–34. [PubMed: 10534749]
25. Pavlova I, Williams M, El-Naggar A, Richards-Kortum R, Gillenwater A. Understanding the biological basis of autofluorescence imaging for oral cancer detection: high-resolution fluorescence microscopy in viable tissue. Clin Cancer Res. 2008; 14:2396–404. [PubMed: 18413830]
26. Roblyer D, Richards-Kortum R, Sokolov K, El-Naggar AK, Williams MD, Kurachi C, et al. Multispectral optical imaging device for in vivo detection of oral neoplasia. J Biomed Opt. 2008; 13:024019. [PubMed: 18465982]
27. De Veld DCG, Witjes MJH, Sterenborg HJCM, Roodenburg JLN. The status of in vivo autofluorescence spectroscopy and imaging for oral oncology. Oral Oncology. 2005; 41:117–31. [PubMed: 15695112]
28. Nitin N, Carlson AL, Muldoon T, El-Naggar AK, Gillenwater A, Richards-Kortum R. Molecular imaging of glucose uptake in oral neoplasia following topical application of fluorescently labeled deoxy-glucose. Int J Cancer. 2009; 124:2634–42. [PubMed: 19173294]
29. Nitin N, Rosbach KJ, El-Naggar A, Williams M, Gillenwater A, Richards-Kortum RR. Optical molecular imaging of epidermal growth factor receptor expression to improve detection of oral neoplasia. Neoplasia. 2009; 11:542–51. [PubMed: 19484143]
30. Holpuch AS, Phelps MP, Desai KG, Chen W, Koutras GM, Han BB, et al. Evaluation of a mucoadhesive fenretinide patch for local intraoral delivery: a strategy to reintroduce fenretinide for oral cancer chemoprevention. Carcinogenesis. 2012; 33:1098–105. [PubMed: 22427354]
31. Mallery SR, Stoner GD, Larsen PE, Fields HW, Rodrigo KA, Schwartz SJ, et al. Formulation and in-vitro and in-vivo evaluation of a mucoadhesive gel containing freeze dried black raspberries: implications for oral cancer chemoprevention. Pharmaceutical research. 2007; 24:728–37. [PubMed: 17372698]
32. Cid YP, Pedrazzi V, de Sousa VP, Pierre MB. In vitro characterization of chitosan gels for buccal delivery of celecoxib: influence of a penetration enhancer. AAPS Pharm Sci Tech. 2012; 13:101–11.
33. Donnelly RF, McCarron PA, Tunney MM, David Woolfson A. Potential of photodynamic therapy in treatment of fungal infections of the mouth. Design and characterisation of a mucoadhesive

patch containing toluidine blue O. Journal of photochemistry and photobiology B, Biology. 2007; 86:59–69.

34. Llabot JM, Manzo RH, Allemandi DA. Double-layered mucoadhesive tablets containing nystatin. AAPS Pharm Sci Tech. 2002; 3:E22.
35. Roblyer D, Kurachi C, Stepanek V, Williams MD, El-Naggar AK, Lee JJ, et al. Objective detection and delineation of oral neoplasia using autofluorescence imaging. Cancer prevention research. 2009; 2:423–31. [PubMed: 19401530]
36. Fang JS, Gillies RD, Gatenby RA. Adaptation to hypoxia and acidosis in carcinogenesis and tumor progression. Semin Cancer Biol. 2008; 18:330–7. [PubMed: 18455429]
37. Liu CG, Zhang L, Jiang Y, Chatterjee D, Croce CM, Huebner K, et al. Modulation of gene expression in precancerous rat esophagus by dietary zinc deficit and replenishment. Cancer Res. 2005; 65:7790–9. [PubMed: 16140947]

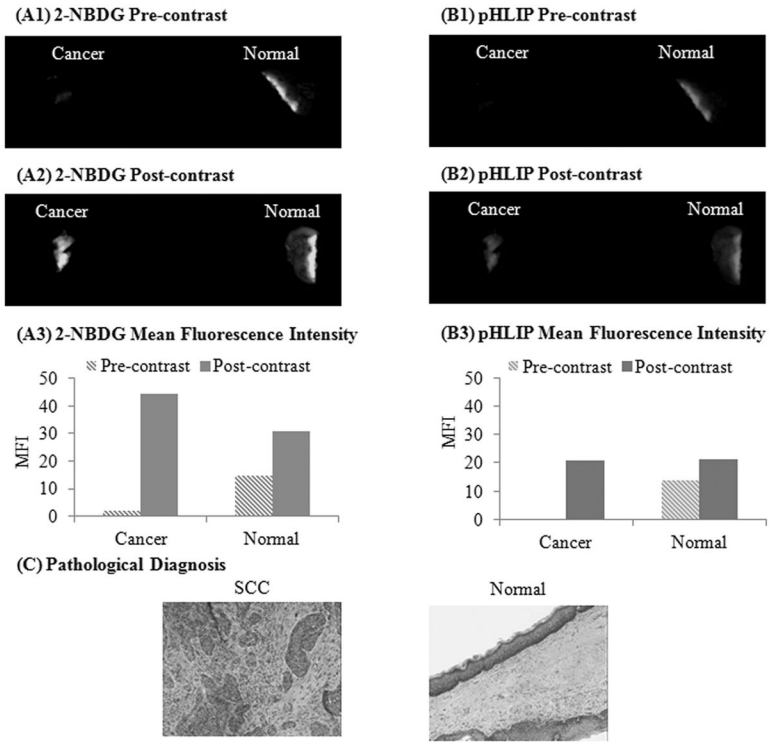

Figure 1.

Illustration of simultaneous imaging of changes in glucose metabolic activity and extracellular pH in clinically isolated paired biopsy specimens. Representative widefield fluorescence images of a paired biopsy set before (pre-contrast) and after (post-contrast) topical application of 2-NBDG (A1, A2) and Alexa 647-pHLIP (B1, B2), respectively. Mean fluorescence intensity of the corresponding pre and post widefield imaging measurements using 2-NBDG (A3) and Alexa 647-pHLIP (B3), respectively. (D) Corresponding pathological H&E images of the paired cancer and normal biopsies.

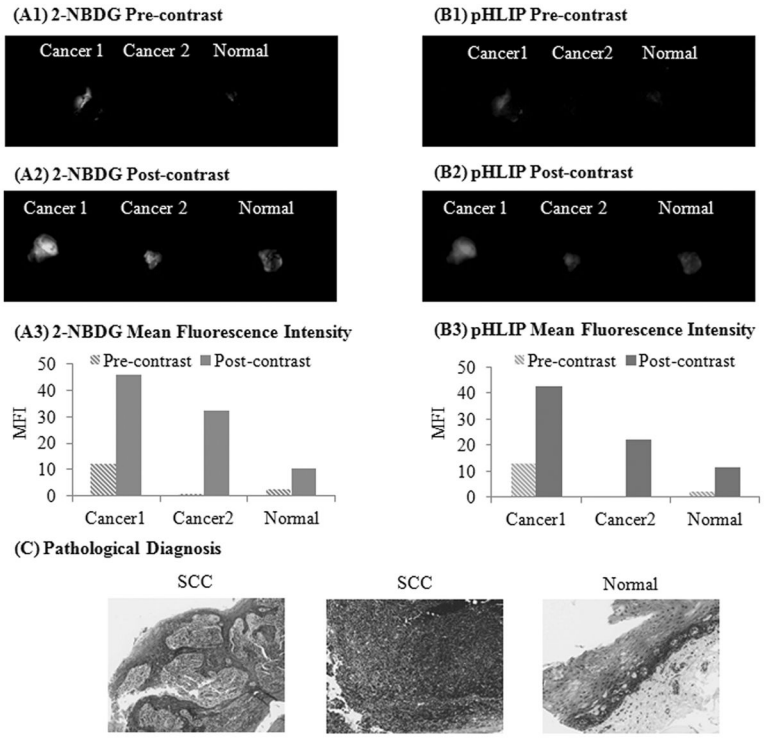

Figure 2.

Changes in contrast properties of clinically abnormal and normal biopsies following topical application of contrast agents was independent of the tissue autofluorescence levels. Representative widefield fluorescence images (pre and post contrast) of a paired biopsy set in which one of the clinically abnormal biopsies (Cancer 1) had a higher level of autofluorescence in both 2-NBDG (A1, A2) and Alexa 647-pHLIP (B1, B2) channels as compared to the paired normal biopsy. Mean fluorescence intensity of the corresponding pre and post widefield imaging measurements using 2-NBDG (A3) and Alexa 647-pHLIP (B3) respectively. (C) Corresponding pathological H&E images of the biopsy set (paired clinically abnormal and normal biopsies).

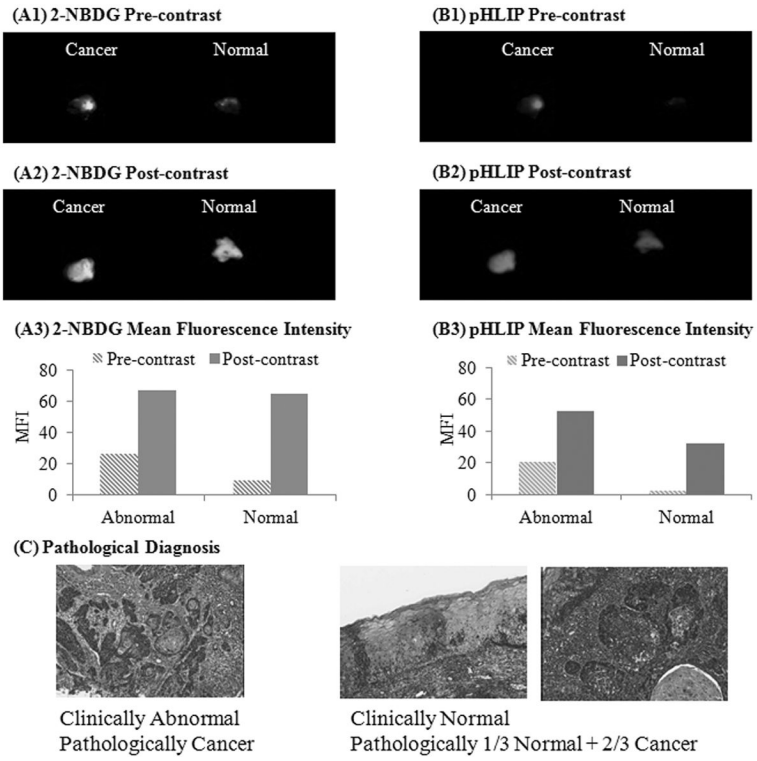

Figure 3.

Sensitivity of 2-NBDG and Alexa 647-pHLIP to detect sub-surface lesions. Widefield fluorescence images of a pair of biopsies before (pre-contrast) and after (post-contrast) topical application of 2-NBDG (A1, A2) and Alexa 647-pHLIP (B1, B2), respectively. Mean fluorescence intensity of corresponding pre and post widefield imaging measurements using 2-NBDG (A3) and Alexa 647-pHLIP (B3), respectively. (C) Corresponding pathological H&E images of the paired clinically normal and abnormal biopsies. In this case, the clinically normal biopsy had an invasive cancer (over 2/3 width) underneath the normal epithelial section.

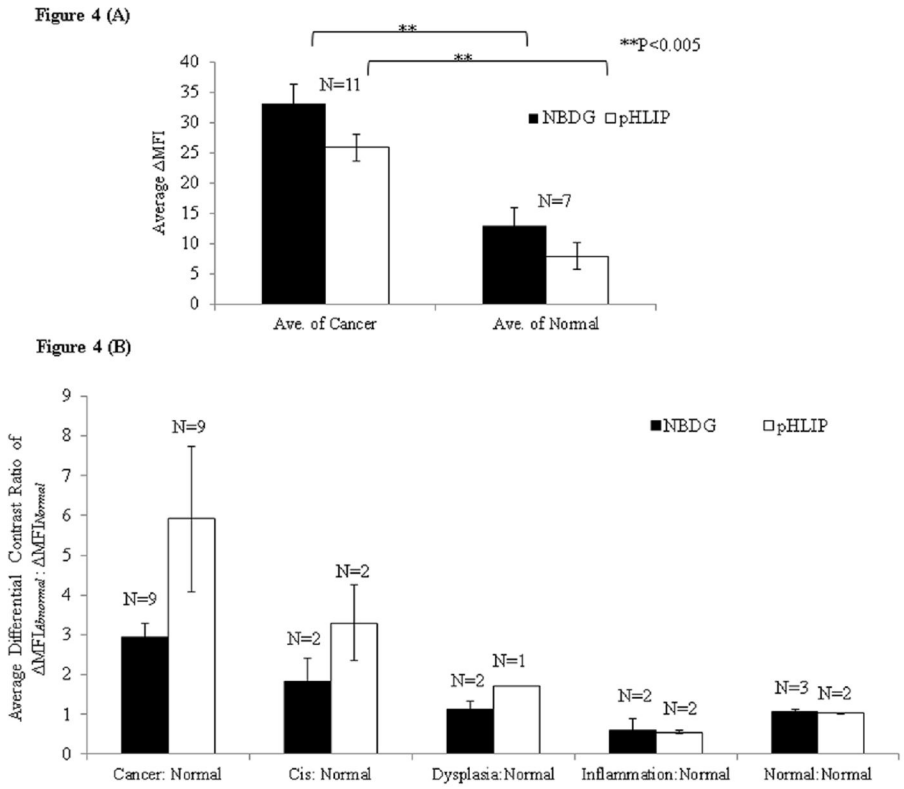

Figure 4.

(A) Average ΔMFI across all cancer and normal biopsy samples before and after topical delivery of 2-NBDG and pHLIP. (B) The comparison of average differential contrast ratios of paired biopsy samples as a function of pathological diagnosis after staining with 2-NBDG and pHLIP respectively.

Table 1

Clinically isolated paired biopsies and their pathological diagnosis

Patient #	Clinically "Abnormal" Location		Pathological Diagnosis	Clinically "Normal" Location		Pathological Diagnosis
1	Tonsil		Invasive Squamous Cell Carcinoma (SCC) (n=9)	Tonsil		Normal
2 A&B	Tonsil			Tonsil		
3 A&B	Tonsil			Tonsil		
4	Tonsil			Base of Tongue		
5	Epiglottis			Post. pharynx		
6	Subglottis			Epiglottis		
7	Hard palate			Buccal		
8 A & B	Base of Tongue		Carcinoma In Situ (Cis) (n=2)	Base of Tongue		
9 A & B	Base of Tongue		Normal (n=3)	Base of Tongue		
10	Base of Tongue			Buccal		
11 A&B	Base of Tongue		Normal with chronic inflammation (n=2)	Base of Tongue		
12	Tonsil		Moderate Dysplasia	Soft palate		
13	Base of Tongue		Mild Dysplasia	Buccal		
14*	Left vallecula		Invasive Squamous Cell Carcinoma (SCC)	Right Base of Tongue		1/3 Normal 2/3 SCC